scientific reports

Check for updates

OPEN

Three-dimensional reconstruction of a biliary system in a bioengineered liver using decellularized scaffold

Hiroshi Horie[1], Ken Fukumitsu[1,2]✉, Yusuke Hanabata[1], Takuma Karasuyama[1], Kentaro Iwaki[1], Fumiaki Munekage[1], Kenta Makino[1], Takashi Ito[1], Katsuhiro Tomofuji[1], Hidenobu Kojima[1], Satoshi Ogiso[1], Elena Yukie Uebayashi[1], Hiroyuki Uematsu[3], Roberto Coppo[3], Kunishige Onuma[3], Masahiro Inoue[3], Takamichi Ishii[1] & Etsuro Hatano[1]

Bioengineered livers are potential alternatives for liver transplantation in patients with end-stage liver disease. Liver scaffolds engineered through decellularization techniques have been developed for clinical applications; however, reconstruction of an integrated biliary system remains a challenge. This study aimed to structurally reconstruct a three-dimensional biliary architecture in bioengineered livers through recellularization of decellularized rat liver scaffolds with rat primary hepatocytes (PHs) and intrahepatic cholangiocyte organoids (ICOs), and to assess bile acid distribution in relation to the reconstructed hepatobiliary architecture. Decellularized rat liver scaffolds were recellularized using rat PHs and green fluorescent protein (GFP)-expressing ICOs. Dissociated ICOs were injected via the bile duct and cultured for 5 days using a perfusion device, followed by PH injection and 2 days of culture. During co-culture, biliary drainage fluid and culture medium were collected to compare total bile acid concentrations using enzyme-linked immunosorbent assay. Histological and immunofluorescence analyses were performed after 7 days of perfusion culture. Histological analyses confirmed the engraftment of GFP-expressing ICOs into bile ducts and PHs into the parenchymal space. Engrafted PHs expressed ZO-1 and MRP2, forming bile canaliculi. In specific regions, MRP2-positive PHs and KRT19-positive ICO-repopulated cells adhered to each other, resembling the native liver structure. In the samples exhibiting such structures, total bile acid concentrations in the biliary drainage fluid tended to be higher than in the culture medium. This study provides evidence supporting the structural reconstruction of a three-dimensional biliary system in bioengineered livers. These findings represent a significant step toward the development of bioengineered livers using decellularization and recellularization techniques.

Keywords Liver regeneration, Tissue engineering, Intrahepatic cholangiocyte organoids, Hepatocytes, Bioartificial organs

Abbreviations

3D	Three-dimensional
BD	Bile duct
ELISA	Enzyme-linked immunosorbent assay
EM	Expansion medium
ESLD	End-stage liver disease
GFP	Green fluorescent protein
ICO	Intrahepatic cholangiocyte organoids
PH	Primary hepatocytes
PV	Portal vein

[1]Division of Hepato-Biliary-Pancreatic Surgery and Transplantation, Department of Surgery, Graduate School of Medicine, Kyoto University, 54 Shogo-in Kawahara-cho, Sakyo-ku, Kyoto 606-8507, Japan. [2]Department of Surgery, Kyoto Katsura Hospital, 17 Yamadahirao-cho, Nisigyo-ku, Kyoto 615-8256, Japan. [3]Department of Clinical Bio-Resource Research and Development, Graduate School of Medicine, Kyoto University, 46-29 Yosida-shimo-adachi-cho, Sakyo-ku, Kyoto 606- 8501, Japan. ✉email: tsurugi@kuhp.kyoto-u.ac.jp

End-stage liver disease (ESLD) causes approximately 2 million deaths annually worldwide[1]. Liver transplantation is the only curative and well-established treatment for patients with ESLD; however, in the United States alone, approximately 2,500 patients with ESLD die annually because of the shortage of donor organs[2]. Various approaches, including cell transplantation, bioartificial organs, and liver support devices, have been investigated to address this challenge[3]; however, none have been successfully established as therapeutic alternatives.

Decellularized liver scaffold-based bioengineering has recently emerged as a promising strategy to address the needs of these patients[4–6]. These scaffolds, composed of extracellular matrix, retains its microvasculature and biological properties, providing a three-dimensional (3D) framework for recellularization with liver cells, such as hepatocytes, cholangiocytes, and endothelial cells[7–16]. In the native liver, coordinated interactions among these cells are crucial for maintaining functional complexity. Bile excretion is facilitated by the connection between the bile canaliculi, which are formed by hepatocytes, and the bile ducts (BDs), which are composed of cholangiocytes. Recent studies have reported that a bile excretion system could be constructed by connecting hepatocytes and cholangiocytes in a two-dimensional culture environment using different cell sources[17,18]. However, a 3D reconstruction of a biliary excretion system has not yet been achieved.

We recently reported that mouse and human intrahepatic cholangiocyte organoids (ICOs) could be potential BD cell sources for recellularization[11]. ICOs, isolated from BD fragments embedded in Matrigel, could be cultured and passaged to maintain cholangiocyte characteristics. Recellularization with ICOs, following dissociation into single cells via the BD of the liver scaffold, can reconstruct the luminal structure of the BDs.

Primary hepatocytes (PHs) are isolated cells that perform essential liver functions, including bile secretion, protein synthesis, and detoxification. Because of their ability to closely mimic the physiological and metabolic activities of the liver tissue, they are widely used for in vitro studies of liver function, drug metabolism, and toxicity. They have also been investigated for recellularization of cell sources. Previous studies have reported that transplantation of recellularized livers with PHs could support liver function in recipients[19,20]. However, the structural and functional integration of hepatocytes within recellularized livers, particularly regarding how these hepatocytes engraft, repolarize, and contribute to bile canaliculi formation, have not been thoroughly investigated.

In this study, we hypothesized that co-recellularization of decellularized liver scaffolds with PHs and ICOs could reconstruct a 3D biliary system in bioengineered livers.

Results

Decellularization of the rat whole liver

A translucent acellular liver scaffold was generated 48 h after decellularization (Fig. 1A). Hematoxylin eosin and Masson's trichrome staining confirmed the absence of nuclei and cytoplasmic components in the decellularized liver scaffold (Fig. 1B). Crystal violet injection of the portal vein (PV) and BD showed that the vascular system remained intact after decellularization (Fig. 1C).

Characteristics of rat ICOs

Rat bile duct fragments were isolated after enzymatic digestion, as shown in Fig. 2A and ICOs proliferated rapidly when cultured in expansion medium (EM) embedded in Matrigel (Fig. 2B, Supplementary Table S1). ICOs in expansion culture were analyzed using immunofluorescence to determine the expression of markers specific to cholangiocytes and hepatocytes. Compared to native liver (Fig. 2C), immunofluorescence analyses revealed that the ICOs expressed cholangiocyte lineage markers KRT19 and SOX9, while the hepatocyte markers ALB and Hnf4a were absent (Fig. 2D). These findings indicate that ICOs cultured under expansion conditions exhibited cholangiocytic characteristics.

Bile canalicular formation in recellularized liver with PHs

Freshly isolated rat PHs (5×10^7 cells) were injected via the BD of the scaffolds, followed by perfusion culture via the PV for 2 days (Fig. 3A–D). The viability of freshly isolated PHs at the time of seeding was $93.5 \pm 1.2\%$ ($n = 16$). When PHs were infused alone, the engraftment efficiency of PHs within the scaffold was $93.0 \pm 2.4\%$ ($n = 8$). Gross examination of recellularized livers infused with PHs alone revealed a non-uniform, patchy distribution of hepatocytes within the scaffold (Fig. 3E). Histological analysis demonstrated appropriate distribution of PHs within the parenchymal space, with some cells engrafted and adherent to each other (Fig. 3F). Immunofluorescence revealed MRP2 and ZO-1 expression on the membrane side of viable hepatocytes, showing patterns similar to those of native liver (Fig. 3G). Electron microscopy confirmed bile canalicular structures between hepatocytes, characterized as a space with microvilli surrounded by tight junctions, similar to the native liver (Fig. 3H).

Reconstruction of biliary structure in recellularized liver with PHs and ICOs

To reconstruct biliary structure, 5×10^6 LDO-derived cells were injected via the BD and perfused with EM via the PV for 5 days. Then, freshly isolated rat PHs (5×10^7 cells) were injected via the BD, followed by perfusion culture with co-culture medium via the PV for 2 days (Fig. 4A). The engraftment efficiency of ICOs was $98.1 \pm 0.6\%$ ($n = 8$), and the engraftment efficiency of PHs after ICO infusion was $92.3 \pm 1.3\%$ ($n = 8$).

Histological analyses revealed the distribution of cells engrafted into the BD lumen and parenchymal space. Immunofluorescence confirmed that GFP-positive cells corresponded to KRT19-positive cells and were distinct from albumin-positive cells (Fig. 4B and C). These results indicate that ICOs reconstructed the BDs and PHs were engrafted in the parenchyma, maintaining their respective characteristics. To further evaluate biliary structure, confocal z-stack images were acquired from 50-µm frozen sections. This analysis demonstrated that KRT19-positive cells engrafted within the bile duct ECM formed continuous duct architectures (Fig. 4D). In addition, electron microscopy revealed microvillus-like structures on the luminal surface of cells reconstructing

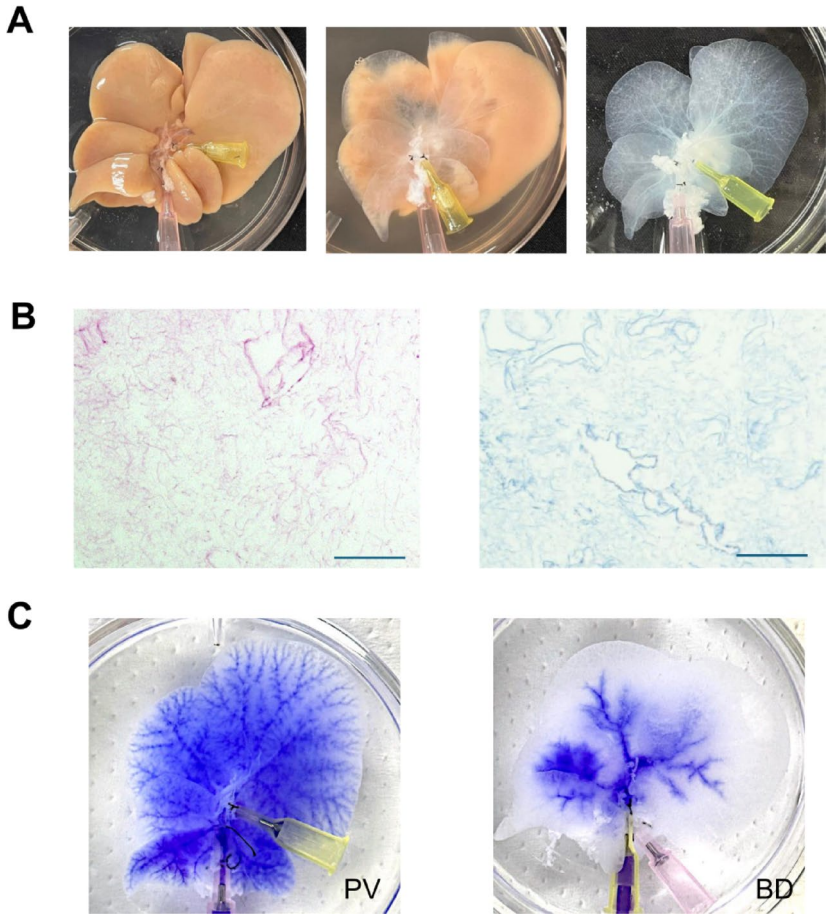

Fig. 1. Characteristics of the decellularized liver scaffold. (**A**) Gross appearance of the rat whole liver during decellularization. (**B**) Hematoxylin and eosin staining and Masson's trichrome staining. (**C**) Intrahepatic portal tree and bile ducts stained with crystal violet. Scale bars = 50 μm. PV, portal vein; BD, bile duct.

ducts (Fig. 4E). Collectively, these observations suggest that ICOs engrafted within the bile duct ECM were repolarized and formed continuous tubular structures.

In some cell clusters, the cells engrafted into the BD and parenchyma adhered to each other (Fig. 4F). In these areas, MRP2 expression in the recellularized PHs was co-localized with KRT19-positive BDs, resembling native liver architecture (Fig. 4G). In addition, confocal fluorescence microscopy for GFP and HNF4α demonstrated that GFP-positive ICOs localized within the bile duct ECM, and HNF4α-positive PHs were positioned in close proximity to these structures (Supplementary Fig. S1).

Bile acid distribution in biliary drainage from recellularized liver

During the 2-day perfusion culture after recellularization of PHs and LDOs, approximately 30–50μL of drainage fluid from the BD was collected using a syringe connected to the culture dish (Fig. 5A).

ELISA for the total bile acids in the biliary drainage and culture medium were performed. In the three samples that exhibited bile canaliculi with MRP2 expression close to the BDs, the total bile acid concentrations in the biliary drainage tended to be higher than in the culture medium (6.35 ± 2.43 vs. 2.59 ± 0.29nmol/10^6cells, $p = 0.100$; Fig. 5B). In contrast, among the five specimens lacking bile canaliculi in proximity to bile ducts, no significant difference in concentration was observed (3.87 ± 1.80 vs. 5.73 ± 2.93nmol/10^6cells, $p = 0.310$) (Supplementary Fig. S2).

Discussion

In this study, rat PHs injected into decellularized liver scaffolds adhered to each other, repolarized, and formed bile canaliculi. Co-recellularization with rat PHs and ICOs enabled the reconstruction of biliary structures, with bile duct structures repopulated by ICOs forming luminal architectures, and bile canaliculi formed by PHs within localized cell clusters. In grafts in which such hepatobiliary structural proximity was observed, total bile acid concentrations in the biliary drainage tended to be higher than those in the perfusing culture medium. Together, these findings support the feasibility of reconstructing key structural elements of a three-dimensional biliary architecture in bioengineered livers using decellularized scaffolds recellularized with rat PHs and ICOs. While the observed bile acid distribution provides preliminary observations related to these reconstructed structures, more comprehensive functional analyses will be required to determine their functional relevance.

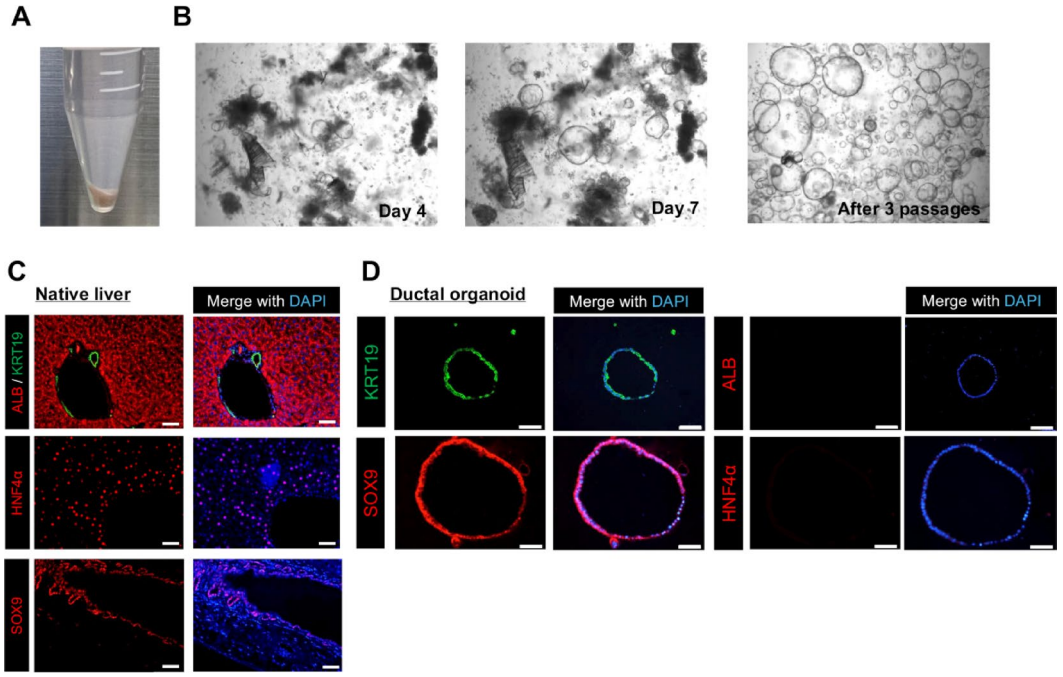

Fig. 2. Isolation, culture, and characteristics of rat intrahepatic cholangiocyte organoids (ICOs). (**A**) Fragments of intrahepatic bile ducts precipitated in a conical tube. (**B**) Images at day 4 (left) and day 7 (middle). After three passages (right), sufficient purification was achieved. (**C**) Immunofluorescence showing hepatocytes positive for albumin and HNF4α, and cholangiocytes positive for KRT19 and SOX9 in the native liver. (**D**) Rat ICOs exhibited cholangiocyte characteristics (KRT19 and SOX9 expression) without hepatocyte characteristics (albumin and HNF4α expression). Scale bars = 50 μm.

Over the past decade, significant advancements have been made in the development of decellularized liver-based bioengineered livers using various recellularized cell sources for clinical applications. Takeishi et al. reported that hepatocytes, cholangiocytes, and vascular endothelial cells derived from human induced pluripotent stem cells successfully recellularized rat liver scaffolds and could be transplanted into immunocompromised rats[12]. Human-specific albumin and A1AT were identified in the serum using ELISA 4 days after transplantation, indicating graft functionality in vivo. In a more clinically relevant study, Higashi et al. reported heterotopic transplantation of porcine recellularized liver grafts with PHs and vascular endothelial cells into porcine liver failure models[19]. Angiography and contrast-enhanced CT on postoperative day 28 confirmed graft perfusion, and serum markers such as total bilirubin, AST, ALT, ALP, and NH_3 were lower in the transplant group than in the control group at most postoperative time points. Despite these developments towards the adoption of bioengineered livers in clinical settings, the biliary system has not been sufficiently addressed.

In this study, we first focused on how the recellularized hepatocytes engrafted onto the scaffold. We demonstrated that rat PHs can repolarize and form bile canaliculi, as shown by ZO-1 and MRP2 expression and transmission electron microscopy at the parenchymal space. These results indicate that the extracellular matrix of the liver scaffold facilitates hepatocyte engraftment and contributes to the formation of bile canaliculi. To the best of our knowledge, this is the first study to demonstrate the reconstruction of bile canalicular structures and their distribution within a recellularized liver.

Two-dimensional reconstruction of a bile excretion system has been reported. Tanimizu et al. co-cultured mouse small hepatocytes and primary cholangiocytes in a two-dimensional culture environment, enabling the development of cell populations, which retained the functional connections of hepatocytes and cholangiocytes[17]. In their study, bilirubin and fluorescein-labeled bile acid were absorbed by hepatocytes, excreted into bile canaliculi, and accumulated in the biliary system. Huang et al. used chemically induced liver progenitors to engineer an integrated tubule-hepatocyte tissue[18]. Chemically induced liver progenitors were generated from mature hepatocytes, differentiated into biliary epithelial cells, and formed biliary duct-like structures. Rat PHs were then plated onto tubular biliary-duct-like structures and cultured for 5 days in two-dimensional culture conditions, resulting in the formation of integrated tubule-hepatocyte tissue with functional interaction between hepatocytes and chemically induced liver progenitor-derived biliary-duct-like structures.

Three-dimensional reconstruction of a bile excretion system in bioengineered livers could significantly contribute not only to the adoption of bioengineered livers in transplantation medicine but also to the field of drug development. Several studies have attempted 3D reconstruction of the biliary system in decellularized liver scaffolds using recellularization techniques[21–23]; however, they did not demonstrate detailed biliary structure, bile canaliculi, and BD, or data suggesting functional reconstruction of the biliary excretion system.

In this study, we used ICOs as recellularization sources for decellularized BDs. We previously reported that ICOs have cholangiocyte characteristics and can efficiently repopulate BDs of the liver scaffold[11]. An advantage

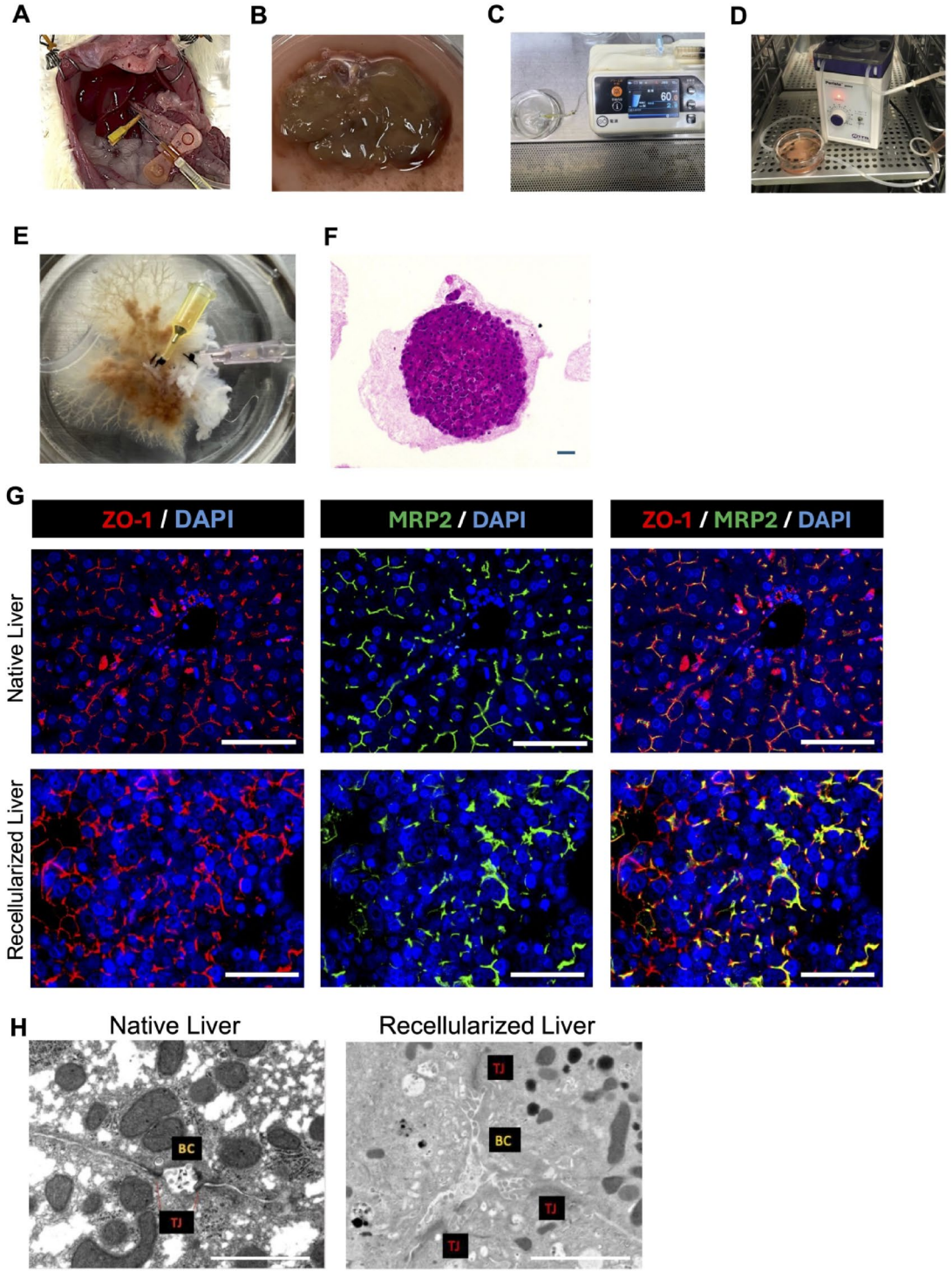

Fig. 3. Recellularization with rat primary hepatocytes (PHs). (**A**) Cannulated rat liver before the two-step collagenase perfusion for primary hepatocyte preparation. (**B**) Extirpated rat liver after the perfusion. (**C**) Injection of isolated PHs into the bile ducts of the decellularized liver at a constant rate using a syringe pump. (**D**) Recellularized liver in a customized chamber connected to a circulation device. (**E**) Representative gross appearance of recellularized liver. (**F**) Hematoxylin and eosin staining of recellularized liver. (**G**) Immunofluorescence of ZO-1 and MRP2 in native liver and recellularized liver. (**H**) Transmission electron microscopy images of the bile canalicular space with microvilli in native and recellularized livers. Scale bars = 50 μm (E–G) and 1 μm (H).

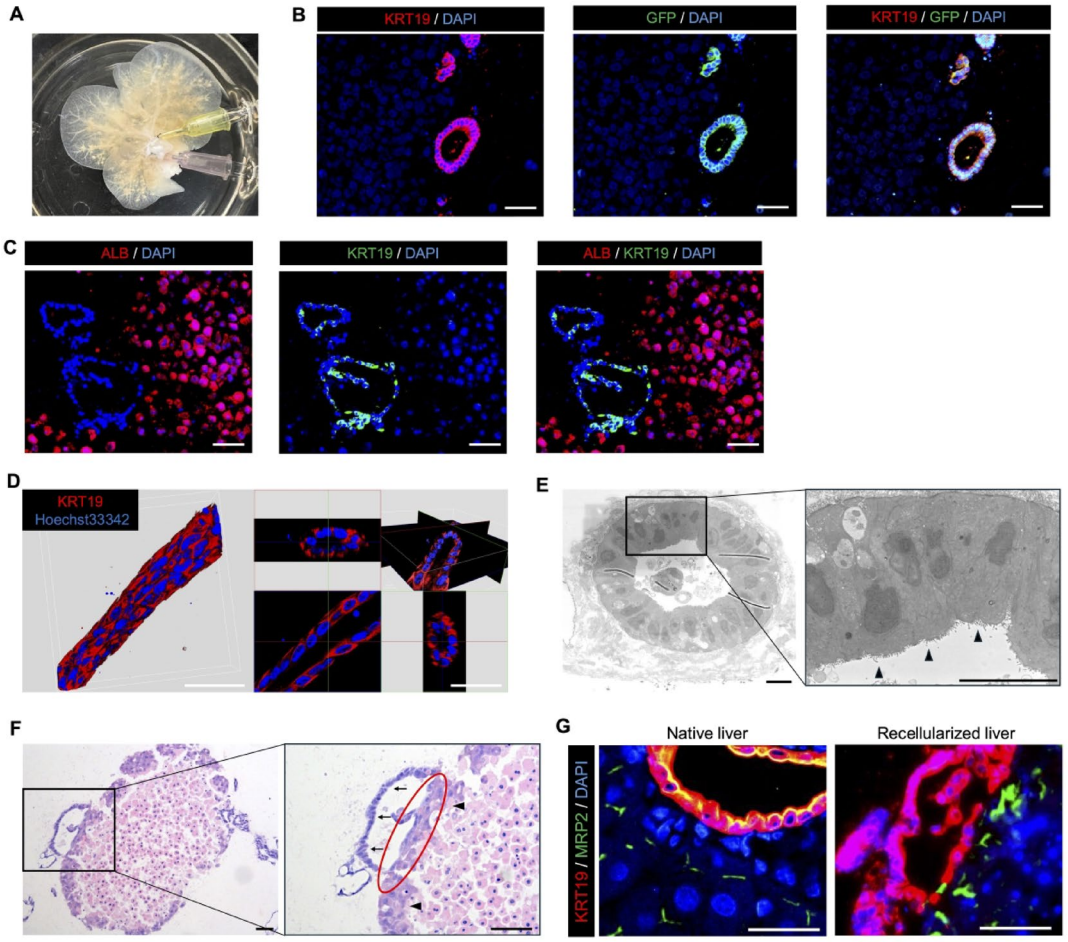

Fig. 4. Recellularization with rat primary hepatocytes (PHs) and intrahepatic cholangiocyte organoids (ICOs). (**A**) Gross appearance of the recellularized liver scaffold with PHs and ICOs. (**B** and **C**) Immunofluorescence staining of recellularized liver sections with indicated antibodies. (**D**) Confocal z-stack imaging and three-dimensional reconstruction of KRT19-positive ductal structures formed within the recellularized bile duct extracellular matrix (left). Orthogonal two-dimensional sections extracted from the z-stack demonstrating the presence of a continuous luminal architecture (right). (**E**) Electron microscopy image showing ICOs engrafted within the bile duct extracellular matrix (left), with microvilli-like structures observed on the luminal surface (right). Arrowheads indicate microvilli-like structures on luminal surface. (**F**) Hematoxylin and eosin staining of a region showing attachment of engrafted PHs and ICO-derived bile ducts, as indicated by the red circle. ICOs and PHs are indicated by arrows and arrowheads, respectively. (**G**) The expression patterns of MRP2 and KRT19 positive cells of native liver (left) and recellularized liver (right). Scale bars = 50 μm (B–D, F, G) and 10 μm (E).

of using ICOs is their genetic stability during long-term expansion, which allows a large cell supply. Another advantage is the potential to overcome immunogenicity, which is a major challenge in transplantation medicine, as ICOs can be isolated from human specimens for BD recellularization[11,24].

We demonstrated that serial recellularization of rat ICOs and PHs successfully generated tissues wherein the BDs repopulated with ICOs were in close proximity to bile canaliculi formed by PHs. A schematic diagram of the reconstructed biliary structure in the recellularized liver is provided in Supplementary Fig. S3.

ICOs adhered to each other and reconstructed luminal architectures within the bile duct ECM. The spatial arrangement of MRP2-positive bile canaliculi and KRT19-positive bile duct was similar to that observed in the native liver, suggesting reconstruction of biliary architecture in the recellularized liver.

There have been no reports on the reconstruction of bioengineered livers with a functional bile excretion system. In vivo, bile is produced by hepatocytes, secreted into bile canaliculi, transported through BDs, and discharged into the intestinal tract. Bile acid concentration is higher in bile than in the bloodstream; thus, if the bile excretion pathway is successfully reconstructed, the concentration of bile acids in BD effluents should be higher than in the circulating medium. Our experiments demonstrated that only specimens where bile canaliculi formed in proximity to BDs showed a tendency toward higher bile acid concentrations in the biliary drainage. To our knowledge, this is the first study to compare bile acid distribution between biliary discharge and perfusing culture medium in bioengineered livers generated from decellularized scaffolds. However, these measurements

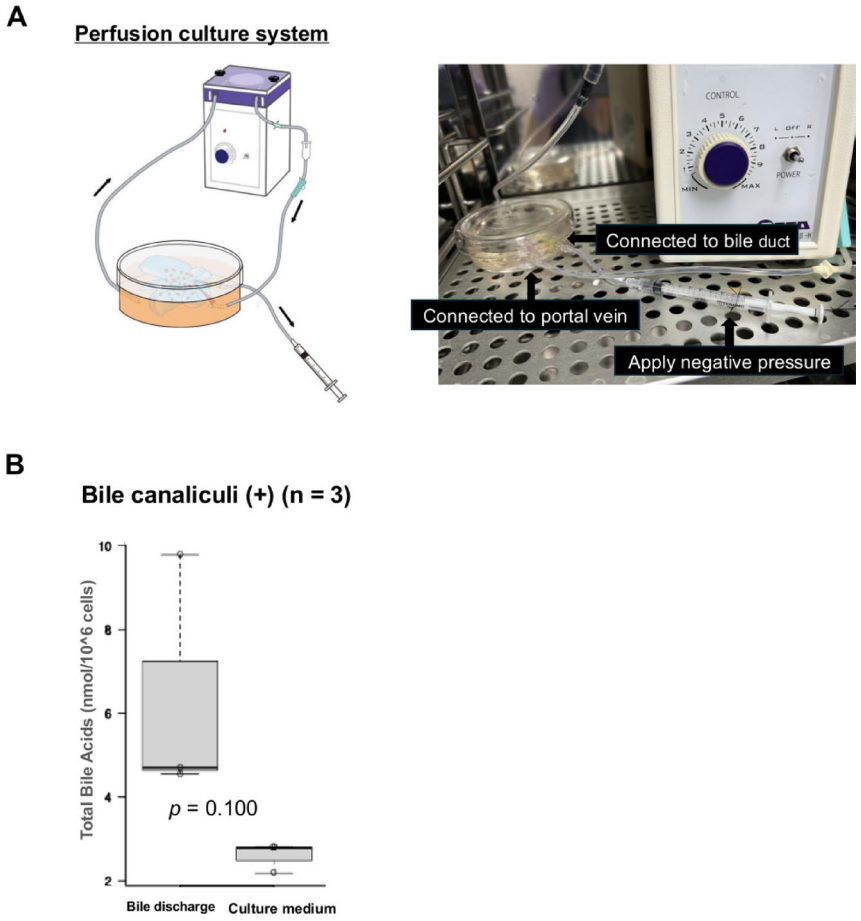

Fig. 5. Comparison of total bile acid concentrations between bile duct discharge and culture medium, with histological correlation. (**A**) Schematic illustration (left) and the actual image (right) showing a system for collecting bile duct discharge. (**B**) Comparison of total bile acids in the culture medium and bile duct discharge. Samples were collected from the cases in which MRP2-positive bile canaliculi were confirmed to be present adjacent to the KRT19-positive bile ducts ($n = 3$, $p = 0.100$). Scale bars = 50 μm.

should be interpreted as preliminary and descriptive, as the volume of recovered biliary samples was limited, precluding analysis of bile components beyond bile acids, and bile acid excretion was not directly observed in real time.

Several limitations of the present study should be acknowledged. First, the current approach does not establish a method to efficiently generate recellularized liver grafts in which bile canaliculi and bile duct structures are consistently located in close proximity. In addition, a subset of hepatocytes located in the central regions of the parenchymal space exhibited enucleated morphology, suggesting suboptimal cell viability or mechanical stress during the recellularization process. Improving recellularization efficiency, spatial organization, and hepatocyte viability will require further optimization of recellularization conditions, including cell numbers and infusion parameters such as pressure and flow. Second, quantitative assessment of graft-wide recellularization was not performed in the present study, including precise estimation of the proportions of recellularized bile duct structures, lobar recellularization, or the frequency at which bile ducts were positioned in close proximity to bile canaliculi. One contributing factor is that, although major tubular ECM structures are preserved after decellularization, it remains technically challenging to reliably distinguish bile duct ECM from other preserved vascular or parenchymal ECM components, or to accurately delineate original hepatic lobar boundaries within decellularized liver sections. Although we attempted unbiased histological evaluation by analyzing multiple sections obtained from all hepatic lobes, recellularized livers form heterogeneous cell populations with non-uniform spatial distribution. Consequently, section-based analyses may provide partial representations of local structural features and may not necessarily reflect global recellularization patterns across the entire graft. From this perspective, comprehensive evaluation of recellularization efficiency would ideally involve wide-field, three-dimensional visualization of cell distribution and biliary structures, potentially leveraging the translucent properties of decellularized scaffolds, to enable more accurate and comprehensive assessment of biliary architecture at the whole-graft level. Another important limitation of the present study is the lack of molecular assessment of cholangiocyte maturation and functional status in the recellularized bile ducts. While structural and ultrastructural analyses demonstrated lumen formation and cellular polarization, these findings do not establish functional maturation of biliary epithelial cells. Comprehensive molecular characterization, including

the expression of cholangiocyte maturation markers and transporters, will therefore be required in future studies to fully evaluate biliary function in this system. Finally, functional assessment in this study remains preliminary as mentioned. Real-time bile excretion was not directly observed, and the limited volume of recovered biliary samples precluded detailed analysis of bile composition beyond bile acids. Future studies will be required to establish real-time bile acid excretion assays and to evaluate biliary function through bile collection using normothermic machine perfusion or transplantation-based models with blood circulation. Ideally, if the bile excretion system in recellularized livers can be successfully reconstructed using autologous hepatocyte sources, it would significantly enhance the clinical potential of bioengineered livers.

In summary, our findings indicate the potential for reconstructing a 3D biliary structure in bioengineered livers generated through recellularization of liver scaffolds with rat PHs and ICOs. While the present study provides structural evidence of biliary reconstruction, further comprehensive functional assessment will be required to determine whether these reconstructed structures support physiological bile excretion.

Methods

Animals

The experimental procedures described in this study were based on the methods reported in our previous publication by Tomofuji et al.[11]. Lewis rats (200–300 g; SLC, Hamamatsu, Japan) were used to prepare the 3D liver scaffolds, PHs, and ICOs. Rats were maintained on a standard laboratory diet with water ad libitum, and were housed in a temperature- and humidity-controlled environment under a constant 12-hour light/dark cycle at the Kyoto University animal facility. Rats used for liver procurement were euthanized by exsanguination under deep isoflurane anesthesia, in accordance with institutional guidelines and approved protocols. All animal experiments were approved by the Kyoto University Animal Experimentation Committee under protocols MedKyo22166 (valid from April 7, 2017 to March 31, 2023) and 24,184 (from April 1, 2023 to March 31, 2025), and were performed in accordance with the Kyoto University Animal Protection Guidelines. The study is reported in accordance with ARRIVE guidelines.

Liver harvest and decellularization

Liver harvest and preparation of decellularized liver scaffolds were performed according to our previous report[10]. Briefly, harvested livers were cannulated with a 24-gauge cannula in the BD and a 20-gauge cannula in the portal vein (PV), and washed with PBS. The livers were frozen at − 80 °C, thawed overnight at 4 °C, then perfused with 0.25% (w/v) Trypsin-1 mmol/L EDTA-4Na solution with phenol red (Wako, Osaka, Japan) at 37 °C for 1 h. This was followed by perfusion with 0.1% polyoxyethylene octyl phenyl ether (Wako, Osaka, Japan) and 0.05% EDTA solution (Sigma, St. Louis, MO, USA) at a flow rate of 0.5 mL/min for 48 h. The decellularized livers were sterilized by perfusion with 0.1% peracetic acid (Sigma-Aldrich, St. Louis, MO, USA) for 2 h and washed with sterilized PBS.

Preparation of cell sources

PHs

Rat PHs were isolated using a two-step collagenase perfusion technique, as previously described[25]. Briefly, Lewis rats were anesthetized with isoflurane (Wako, Osaka, Japan) and the PV was cannulated with a 25-gauge needle. After cutting the suprahepatic and infrahepatic inferior vena cava, the liver was perfused with 50mL of Ca^{2+}-free HBSS containing 0.5 mM EGTA (Wako, Osaka, Japan) and 2 U/mL heparin (Novo-Heparin; Mochida, Tokyo, Japan) for 5 min, followed by 50 mL of collagenase solution containing 0.15% dispase II (Sanko Junyaku, Tokyo, Japan), 0.15% collagenase type II (Gibco, Palo Alto, CA, USA), 0.1 mg/mL DNase I (from bovine pancreas, Sigma, St.Louis, MO, USA), heparin 2 U/mL, 150 mmol/L NaCl, 5.4 mmol/L KCl, 0.34 mmol/L $NaHPO_4$, 0.1 mmol/L $MgSO_4$, 5.0 mmol/L $CaCl_2$, 4.2 mmol/L $NaHCO_3$, 5.6 mmol/L glucose, and 10 mmol/L HEPES (all of the chemical reagents other than those indicated were purchased from Wako) for 10 min at 37 °C. The liver was resected, gently shaken to dissociate cells, and filtered through a 100 µm strainer (BD Falcon, Franklin Lakes, NJ, USA). The suspension was washed three times by centrifugation at 50 × g for 3 min at 4 °C. Isolated PHs were immediately used for recellularization. Hepatocyte viability was assessed by trypan blue exclusion using a hemocytometer prior to scaffold infusion, and only cell preparations with viability > 90% were used for subsequent experiments.

Green fluorescent protein (GFP)-expressing ICOs

Rat ICOs were prepared and cultured as previously reported in mice[11] with modifications. Briefly, the left lateral lobe of the liver was harvested from Lewis rats, mechanically minced with scissors into approximately 2–3 mm cubes, and serially passed through 18-, 20-, 22-, and 23-gauge needles for mechanical fragmentation. Then, fragments were enzymatically digested with 2.6 µU/mL Liberase DH (Roche, Basel, Switzerland) in DMEM (Wako, Osaka, Japan) containing 0.1 mg/mL DNase I (Sigma-Aldrich, St. Louis, MO, USA) for 10 min at 37 °C. The digested fragments were serially passed through 100 and 40 µm mesh filters. Collected clusters were suspended in DMEM (Wako, Osaka, Japan), centrifuged at 440 × g for 3 min, and the pelleted cell clusters were suspended in Matrigel-GFR (Corning, NY, USA) at approximately 20–30 clusters per 7 µL on non-treated culture plates (IWAKI, AGC Techno Glass, Shizuoka, Japan). After gelation of the Matrigel at 37 °C for 10 min, tissue fragments were cultured with EM for 5–7 days until the emergence of organoids. Established organoids were passaged every 4–6 days by dispersion using TrypLE Express (Invitrogen, Carlsbad, CA, USA) at 37 °C for 15 min, and re-embedded in Matrigel-GFR for further culture or recellularization.

The pLX304-GFP, a GFP-expressing lentiviral vector, was generated by transferring a GFP-coding sequence from pALB-GFP (#55759; Addgene, Watertown, MA, USA) to pENTR4 (#17424; Addgene, Watertown, MA, USA), followed by gateway cloning into pLX304 (#25890; Addgene, Watertown, MA, USA). Lentiviral particles

were generated in HEK293FT cells co-transfected with pLX304-GFP, psPAX2 (#12260; Addgene, Watertown, MA, USA), and pMD2G (#12259; Addgene, Watertown, MA, USA) using X-tremeGENE™ HD (Roche, Basel, Switzerland) following the instructions of the manufacturer. Viral supernatants were harvested at 48 and 72 h post-transfection, and filtered through a 0.45 μm PVDF membrane (Merck Millipore, Burlington, MA, USA). For lentiviral infection, ICOs were dissociated into single cells and mixed with filtered viral supernatant. The cell-lentivirus mixture was supplemented with 10 μM Y27632 (LC Laboratories, Woburn, MA, USA), 1mM N-acetyl-L-cysteine (Wako, Osaka, Japan), and 10 μg/mL, polybrene (Sigma-Aldrich, St Lois, MO, USA), transferred to an untreated plate and centrifuged at 2000 rpm for 1 h at room temperature. After centrifugation, the supernatant was discarded, and the cells were embedded in Matrigel drops and cultured in EM. After expansion, organoids were passaged and selected using blasticidin (Wako, Osaka, Japan).

Recellularization and perfusion culture of rat whole liver

Perfusion culture of recellularized liver with only PHs

A total of 5.0×10^7 PHs suspended in 30 ml of medium based on HCM™ (Lonza Sales Ltd., Basel, Switzerland) supplemented with 10% FBS were injected via the BD of the liver scaffolds at a constant flow rate of 1mL/min using a syringe pump (JMS Co., Ltd., Hiroshima, Japan). During cell infusion, the syringe pump display was continuously monitored to ensure that the stepwise pressure indicator did not increase. To assess the engraftment efficiency, perfusate leaking from the scaffold during cell infusion was collected, centrifuged at 50 × g for 3 min at 4 °C, and the number of non-engrafted cells was quantified by cell counting. The recellularized liver was incubated at 37 °C for 3 h. After static culture, the recellularized liver was connected to the circulation culture system via the PV cannula and perfused with the medium based on HCM™ supplemented with 10% FBS, 100 U/mL penicillin and 100 μg/mL streptomycin using a peristaltic pump (Perista pump, ATTO Corporation, Tokyo, Japan) at a rate of 0.7–1.0 mL/min at 37 °C. The perfusate was drained from the inferior vena cava and recycled back into the system. Perfusion culture was continued for 48 h.

Perfusion culture of recellularized liver with LDOs and PHs

Single-cell dissociated ICOs (5×10^6 cells) suspended in 5 ml of EM were injected into the liver scaffold via the BD at a constant flow rate of 1 mL/min using the syringe pump. To assess engraftment efficiency, perfusate leaking from the scaffold during and immediately after cell infusion was collected, centrifuged at 440 × g for 3 min at 4 °C, and the number of non-engrafted cells was quantified by cell counting. The recellularized liver was incubated with EM for 3 h and connected to the circulatory system as described above. EM was changed every other day, and perfusion culture was performed for 5 days. Subsequently, 5.0×10^7 rat PHs suspended in 30 ml of co-culture medium (Supplementary Table S2) were injected via the BD. Engraftment efficiency was assessed as described above by collecting leaked perfusate and quantifying non-engrafted cells. After 3 h of static culture, perfusion culture was resumed using the co-culture medium and incubated for another 48 h.

Collection of drainage fluids from the BD

During perfusion culture, the BD of the scaffolds recellularized with PH and ICO was connected to a syringe via a culture dish, and negative pressure was applied by pulling the plunger of the 1 mL syringe and securing it with a thread.

Histological analysis

Organoids were retrieved from Matrigel, re-embedded in Cellmatrix Type I-A (Nitta Gelatin, Osaka, Japan), and fixed overnight in 10% formalin (Wako, Osaka, Japan) at room temperature. Recellularized liver grafts were fixed in 4% paraformaldehyde (Wako, Osaka, Japan) for 24 h at 4 °C and embedded in paraffin.

Paraffin-embedded sections (4 μm) were dewaxed, rehydrated, and subjected to either hematoxylin and eosin staining or immunohistochemistry. For immunostaining, antigen retrieval was performed by autoclaving at 121 °C for 15 min. Sections were incubated in PBS containing 10% donkey or goat serum and 0.1% Triton X-100 (Nacalai Tesque Inc, Kyoto, Japan). Primary antibodies were diluted with PBS, 5% donkey or goat serum, and 0.1% Triton X-100, incubated overnight at 4 °C, followed by secondary antibody incubation for 1 h at room temperature. Sections were mounted with ProLong™ Gold Antifade Mountant with DAPI (Invitrogen, Carlsbad, CA, USA) and visualized using an Olympus BX50F4 microscope (Olympus Optical, Tokyo, Japan).

For frozen section preparation, grafts fixed in 4% paraformaldehyde were sequentially cryoprotected in 10%, 20%, and 30% sucrose solutions (each for 24 h at 4 °C), embedded in cryomolds (Sakura Finetek Japan Co., Ltd., Tokyo, Japan) using OCT compound (Sakura Finetek Japan Co., Ltd.), and stored at − 80 °C. Frozen sections (50 μm) were cut using a cryostat. For immunostaining of frozen sections, the same blocking solution and antibody dilution buffers as used for paraffin sections were applied, and blocking, primary antibody incubation, and secondary antibody incubation were all performed overnight at 4 °C. Sections were counterstained with Hoechst 33,342 (Thermo Fisher Scientific, Waltham, MA, USA) for 30 min at room temperature and imaged using a confocal microscope (Leica Microsystems, Wetzlar, Germany).

For each specimen, five slides were prepared from all hepatic lobes and examined to ensure unbiased evaluation of histological findings. Antibodies used are listed in Supplementary Table S3.

Electron microscopy

Electron microscopy was performed as previously described[8]. Normal fresh livers and decellularized livers of Lewis rats were fixed with 2% glutaraldehyde (Nacalai Tesque Inc, Kyoto, Japan) and 4% PFA in PBS overnight at 4 °C. Samples were microdissected, dehydrated with ethanol (50, 60, 70, 80, 90, 99, and 100%), immersed in t-butanol, frozen at -20 °C, and sublimated. After sputter-coating with a platinum–palladium alloy using an ion

coater (JBC-3000FC, JEOL, Tokyo, Japan), the samples were examined using a scanning electron microscope (JSM-7900 F, JEOL, Tokyo, Japan).

Enzyme-linked immunosorbent assay (ELISA) of total bile acids

After 48 h of perfusion culture of scaffolds recellularized with PHs and LDOs, culture medium and BD drainage fluids were collected. Total bile acid concentrations in both samples were measured using a Total Bile Acids Assay Kit (Cell Biolabs, San Diego, CA, USA) via ELISA. Background bile acid concentrations derived from FBS were measured in medium alone and subtracted from the values obtained for all samples. Bile acid concentrations were normalized to the number of engrafted hepatocytes (per 10^6 cells).

Statistical methods

Data are expressed as mean ± standard error of the mean. Statistical analyses were performed using R version 4.1.0 (R Foundation for Statistical Computing, Vienna, Austria). Statistical significance was defined as $p < 0.05$. Total bile acid concentrations were compared using the non-parametric Mann–Whitney U test. All data points represent independent recellularized liver grafts.

Data availability

The data that support the findings of this study are available from the corresponding author, K.F., upon reasonable request.

Received: 19 September 2025; Accepted: 3 February 2026
Published online: 10 February 2026

References

1. Asrani, S. K., Devarbhavi, H., Eaton, J. & Kamath, P. S. Burden of liver diseases in the world. *J. Hepatol.* **70**, 151–171. https://doi.org/10.1016/j.jhep.2018.09.014 (2019).
2. Nicolas, C. T. et al. Concise review: liver regenerative medicine: from hepatocyte transplantation to bioartificial livers and bioengineered grafts. *Stem Cells*. **35**, 42–50. https://doi.org/10.1002/stem.2500 (2017).
3. Bhatia, S. N., Underhill, G. H., Zaret, K. S. & Fox, I. J. Cell and tissue engineering for liver disease. *Sci. Transl Med.* **6**, 245sr2. https://doi.org/10.1126/scitranslmed.3005975 (2014).
4. Uygun, B. E. et al. Organ reengineering through development of a transplantable recellularized liver graft using decellularized liver matrix. *Nat. Med.* **16**, 814–820. https://doi.org/10.1038/nm.2170 (2010).
5. Soto-Gutierrez, A. et al. A whole-organ regenerative medicine approach for liver replacement. *Tissue Eng. Part. C Methods*. **17**, 677–686. https://doi.org/10.1089/ten.TEC.2010.0698 (2011).
6. Baptista, P. M. et al. The use of whole organ decellularization for the generation of a vascularized liver organoid. *Hepatology* **53**, 604–617. https://doi.org/10.1002/hep.24067 (2011).
7. Chen, C. et al. Hepatocyte-like cells generated by direct reprogramming from murine somatic cells can repopulate decellularized livers. *Biotechnol. Bioeng.* **115**, 2807–2816. https://doi.org/10.1002/bit.26784 (2018).
8. Kojima, H. et al. Establishment of practical recellularized liver graft for blood perfusion using primary rat hepatocytes and liver sinusoidal endothelial cells. *Am. J. Transpl.* **18**, 1351–1359. https://doi.org/10.1111/ajt.14666 (2018).
9. Minami, T. et al. Novel hybrid three-dimensional artificial liver using human induced pluripotent stem cells and a rat decellularized liver scaffold. *Regen Ther.* **10**, 127–133. https://doi.org/10.1016/j.reth.2019.03.002 (2019).
10. Ogiso, S. et al. Efficient recellularisation of decellularised whole-liver grafts using biliary tree and foetal hepatocytes. *Sci. Rep.* **6**, 35887. https://doi.org/10.1038/srep35887 (2016).
11. Tomofuji, K. et al. Liver ductal organoids reconstruct intrahepatic biliary trees in decellularized liver grafts. *Biomaterials* **287**, 121614. https://doi.org/10.1016/j.biomaterials.2022.121614 (2022).
12. Takeishi, K. et al. Soto-Gutierrez, assembly and function of a bioengineered human liver for transplantation generated solely from induced pluripotent stem cells. *Cell. Rep.* **31**, 107711. https://doi.org/10.1016/j.celrep.2020.107711 (2020).
13. Lewis, P. L. et al. Complex bile duct network formation within liver decellularized extracellular matrix hydrogels. *Sci. Rep.* **8**, 12220. https://doi.org/10.1038/s41598-018-30433-6 (2018).
14. Chen, J., Devalliere, Bulutoglu, B., Yarmush, M. L. & Uygun, B. E. Repopulation of intrahepatic bile ducts in engineered rat liver grafts. *Technol. (Singal World Sci)*. **7**, 46–55. https://doi.org/10.1142/S2339547819500043 (2019).
15. Ko, I. K. et al. Bioengineered transplantable Porcine livers with re-endothelialized vasculature. *Biomaterials* **40**, 72–79. https://doi.org/10.1016/j.biomaterials.2014.11.027 (2015).
16. Zhou, P. et al. Decellularization and recellularization of rat livers with hepatocytes and endothelial progenitor cells. *Artif. Organs*. **40**, E25–E38. https://doi.org/10.1111/aor.12645 (2016).
17. Tanimizu, N. et al. Generation of functional liver organoids on combining hepatocytes and cholangiocytes with hepatobiliary connections ex vivo. *Nat. Commun.* **12**, 3390. https://doi.org/10.1038/s41467-021-23575-1 (2021).
18. Huang, Y. et al. Bioengineering of a CLiP-derived tubular biliary-duct-like structure for bile transport in vitro. *Biotechnol. Bioeng.* **118**, 2572–2584. https://doi.org/10.1002/bit.27773 (2021).
19. Higashi, H. et al. Transplantation of bioengineered liver capable of extended function in a preclinical liver failure model. *Am. J. Transpl.* **22**, 731–744. https://doi.org/10.1111/ajt.16928 (2022).
20. Anderson, B. D. et al. Functional characterization of a bioengineered liver after heterotopic implantation in pigs. *Commun. Biol.* **4**, 1157. https://doi.org/10.1038/s42003-021-02665-2 (2021).
21. Hirukawa, K. et al. Novel approach for reconstruction of the three-dimensional biliary system in decellularized liver scaffold using hepatocyte progenitors. *PLOS One*. **19**, e0297285. https://doi.org/10.1371/journal.pone.0297285 (2024).
22. Chen, J. et al. Generation and metabolomic characterization of functional ductal organoids with biliary tree networks in decellularized liver scaffolds. *Bioact Mater.* **26**, 452–464. https://doi.org/10.1016/j.bioactmat.2023.03.012 (2023).
23. Krüger, M. et al. High level of polarized engraftment of Porcine intrahepatic cholangiocyte organoids in decellularized liver scaffolds. *J. Cell. Mol. Med.* **26**, 4949–4958. https://doi.org/10.1111/jcmm.17510 (2022).
24. Willemse, J. et al. Scaffolds obtained from decellularized human extrahepatic bile ducts support organoids to Establish functional biliary tissue in a dish. *Biotechnol. Bioeng.* **118**, 836–851. https://doi.org/10.1002/bit.27613 (2021).
25. Kita, S. et al. The protective effect of transplanting liver cells into the mesentery on the rescue of acute liver failure after massive hepatectomy. *Cell. Transpl.* **25**, 1547–1559. https://doi.org/10.3727/096368916X690999 (2016).

Acknowledgements
We thank the Division of Electron Microscopic Study, Center for Anatomical Studies, Graduate School of Medicine, Kyoto University, for technical assistance with the analysis of electron microscopy data.

Author contributions
Conceptualization: Ken Fukumitsu. Data curation: Hiroshi Horie, Ken Fukumitsu, Yusuke Hanabata, Takuma Karasuyama, Kentaro Iwaki, Fumiaki Munekage, Kenta Makino, Takashi Ito, Katsuhiro Tomofuji, Hiroyuki Uematsu, Robert Coppo, Kunishige Onuma, Masahiro Inoue. Funding acquisition : Hiroshi Horie, Ken Fukumitsu. Investigation : Hiroshi Horie, Ken Fukumitsu, Yusuke Hanabata, Takuma Karasuyama, Kentaro Iwaki, Fumiaki Munekage, Kenta Makino, Takashi Ito, Katsuhiro Tomofuji, Hidenobu Kojima, Satoshi Ogiso, Elena Yukie Uebayashi, Hiroyuki Uematsu, Robert Coppo, Kunishige Onuma, Masahiro Inoue, Takamichi Ishii, Etsuro Hatano. Project administration : Ken Fukumitsu. Resources: Hiroshi Horie, Ken Fukumitsu, Masahiro Inoue. Supervision : Masahiro Inoue, Takamichi Ishii, Etsuro Hatano. Writing—original graft: Hiroshi Horie, Ken Fukumitsu. Writing—review and editing: Satoshi Ogiso, Masahiro Inoue, Takamichi Ishii, Etsuro Hatano.

Funding
This work was supported by JSPS KAKENHI [grant numbers 22K08689, 24KJ1416].

Declarations

Competing interests
The authors declare no competing interests.

Additional information
Supplementary Information The online version contains supplementary material available at https://doi.org/10.1038/s41598-026-39175-2.

Correspondence and requests for materials should be addressed to K.F.

Reprints and permissions information is available at www.nature.com/reprints.

Publisher's note Springer Nature remains neutral with regard to jurisdictional claims in published maps and institutional affiliations.

Open Access This article is licensed under a Creative Commons Attribution-NonCommercial-NoDerivatives 4.0 International License, which permits any non-commercial use, sharing, distribution and reproduction in any medium or format, as long as you give appropriate credit to the original author(s) and the source, provide a link to the Creative Commons licence, and indicate if you modified the licensed material. You do not have permission under this licence to share adapted material derived from this article or parts of it. The images or other third party material in this article are included in the article's Creative Commons licence, unless indicated otherwise in a credit line to the material. If material is not included in the article's Creative Commons licence and your intended use is not permitted by statutory regulation or exceeds the permitted use, you will need to obtain permission directly from the copyright holder. To view a copy of this licence, visit http://creativecommons.org/licenses/by-nc-nd/4.0/.

© The Author(s) 2026